Ground states of atomic Fermi gases in a two-dimensional optical lattice with and without population imbalance

Lin Sun [1] and Qijin Chen [2,3,4,*]

[1] *School of Physics and Zhejiang Institute of Modern Physics, Zhejiang University, Hangzhou, Zhejiang 310027, China*
[2] *Hefei National Research Center for Physical Sciences at the Microscale and School of Physical Sciences, University of Science and Technology of China, Hefei, Anhui 230026, China*
[3] *Shanghai Research Center for Quantum Science and CAS Center for Excellence in Quantum Information and Quantum Physics, University of Science and Technology of China, Shanghai 201315, China*
[4] *Hefei National Laboratory, University of Science and Technology of China, Hefei 230088, China*

(Received 9 May 2022; accepted 14 July 2022; published 25 July 2022)

We study the ground-state phase diagram of population balanced and imbalanced ultracold atomic Fermi gases with a short-range attractive interaction throughout the crossover from BCS to Bose-Einstein condensation (BEC), in a two-dimensional (2D) optical lattice comprised of a 2D array of 1D lines. We find that the mixing of lattice and continuum dimensions, together with population imbalance, has an extraordinary effect on pairing and the superfluidity of atomic Fermi gases. In the balanced case, the superfluid ground state prevails over the majority of the phase space. However, for relatively small lattice hopping integral t and large lattice constant d, a pair density wave (PDW) emerges unexpectedly at intermediate coupling strength, and the nature of the in-plane and overall pairing changes from particlelike to holelike in the BCS and unitary regimes, associated with an abnormal increase in the Fermi volume with the pairing strength. In the imbalanced case, the stable polarized superfluid phase shrinks to only a small portion of the entire phase space spanned by t, d, imbalance p, and interaction strength U, mainly in the bosonic regime of low p, moderately strong pairing, relatively large t, and small d. Due to the Pauli exclusion between paired and excessive fermions within the confined momentum space, a PDW phase emerges and the overall pairing evolves from particlelike into holelike, as the pairing strength grows stronger in the BEC regime. In both cases, the ground-state property is largely governed by the Fermi surface topology. These findings are very different from the cases of a pure 3D continuum, a 3D lattice, or a 1D optical lattice.

DOI: 10.1103/PhysRevA.106.013317

I. INTRODUCTION

Ultracold Fermi gases have provided an ideal platform for investigating the pairing and superfluid physics over the past decades, primarily owing to the high tunability of multiple parameters [1,2]. Using a Feshbach resonance [3], one can tune the effective pairing strength from the weak-coupling BCS limit all the way through to the strong-pairing Bose-Einstein condensation (BEC) limit. There have been a great number of experimental and theoretical studies on ultracold Fermi gases in recent years, with many tunable parameters which have been made accessible experimentally, including pairing interaction strength [1], population imbalance [4–12], and dimensionality [13–15]. In particular, ultracold Fermi gases in an optical lattice exhibit rich physics due to the tunable geometry [16–18]. As is well known, population imbalance suppresses or destroys superfluidity in three-dimensional (3D) homogeneous systems [9,19]. For example, superfluidity at zero temperature is completely destroyed at unitarity and in the BCS regime, whereas stable polarized superfluid (PSF) with a finite imbalance p exists only in the BEC regime [19]. Meanwhile, in the absence of population imbalance in a 3D lattice, one finds the superfluid transition temperature $T_c \propto -t^2/U$ in the BEC regime, due to virtual pair unbinding in the pair hopping process [20,21], which makes it hard to reach the superfluid phase in the BEC regime. (Here t is the lattice hopping integral and $U < 0$ is the on-site attractive interaction.) While the superfluid transition for both population balanced and imbalanced Fermi gases have been realized experimentally in the 3D continuum case (often in a trap), it has not been realized even for the balanced case in 3D lattices. However, superfluidity, long-range or Berezinskii-Kosterlitz-Thouless–like [22], and pairing phenomena have been explored experimentally in 2D and 1D optical lattices [23–28] or quasi-2D traps [29–35]. Common to these experiments is the presence of one or two continuum dimensions. Until a further breakthrough is made in cooling techniques, the presence of continuum dimensions seems to be crucial for the superfluid phase to be accessible experimentally so far in low-dimensional optical lattices (and quasi-2D traps) besides the 3D continuum. We note, however, that these optical lattice experiments have mostly been restricted to the small-t limit such that the coupling between different pancakes (2D planes) or cigar-shaped tubes (1D lines) is negligible. Therefore, a systematic investigation of the vast

*Corresponding author: qchen@uchicago.edu

unexplored parameter space of the low-dimensional optical lattices is important in order to uncover possible exotic and interesting new quantum phenomena.

In the presence of population imbalance, an open Fermi surface of Fermi gases in a one-dimensional optical lattice (1DOL), caused by large lattice constant d and/or small hopping t, often leads to destruction of the superfluid ground state in the BEC regime [36]. Our recent study on pairing and superfluidity of atomic Fermi gases in a 2DOL, which is comprised of two lattice and one continuum dimensions, reveals that for relatively large d and small t, a pair density wave (PDW) ground state emerges in the regime of intermediate pairing strength, and the nature of the in-plane and overall pairing changes from particlelike to holelike in the unitary and BCS regimes, with an unexpected nonmonotonic dependence of the chemical potential on the pairing strength [37].

In this paper we focus on the ground-state superfluid behavior of atomic Fermi gases in a 2DOL, under the effects of lattice-continuum mixing, population imbalance, and its interplay with the lattice parameters. We first investigate the evolution of the Fermi surface as a function of hopping integral t and lattice constant d and then calculate the zero-T superfluid phase diagram using the BCS-Leggett mean-field equations [38] but supplemented with various stability conditions, including those derived from finite-temperature formalism [9]. We explore the superfluid phase diagrams in various phase planes, as a function of lattice constant, hopping integral, and interaction strength for population balanced cases and also of polarization for population imbalanced cases.

We find that in the population balanced case, while the phase diagram at zero T is dominated by the superfluid phase, a PDW ground state may emerge at intermediate pairing strength, for relatively small t and large d, and the nature of the in-plane and overall pairing changes from particlelike to holelike in the BCS and unitary regimes. This is associated with an open Fermi surface, where the effective number density in the lattice dimensions can go above half filling. The PDW state originates from strong interpair repulsive interactions and relatively large pair size at intermediate pairing strength, which is also found in dipolar Fermi gases within the pairing fluctuation theory [39].

In the population imbalanced case, due to the constraint of various stability conditions, stable superfluid ground states are found to exist only in a small portion of the multidimensional phase space, spanned by the parameters t, d, p, and U, mainly in the low-p and bosonic regime of intermediate pairing strength, and for relatively large t and small d. As the pairing interaction becomes stronger in the BEC regime, the nature of the overall pairing of a polarized Fermi gas in a 2DOL evolves from particlelike into holelike. As manifested in the momentum distribution of the paired fermions and excessive majority fermions, there is a strong Pauli exclusion between them for small t and large d. Therefore, decreasing t and increasing d and p help extend the holelike pairing regime toward weaker coupling. These results are very different from their counterparts in pure 3D continua, 3D lattices, and 1DOLs.

We mention that the values of t and d for which one finds holelike pairing in the weaker-coupling regime in the balanced case and in the stronger-coupling regime in the imbalanced case do not overlap. This can be understood as the balanced case and the $p \to 0^+$ case are not continuously connected at $T = 0$.

II. THEORETICAL FORMALISM

A. General theory

Here we consider a two-component ultracold Fermi gas with a short-range pairing interaction, $V_{\mathbf{k},\mathbf{k}'} = U < 0$, in a 2DOL. The dispersion of noninteracting atoms without population imbalance is given by $\xi_{\mathbf{k}} = \epsilon_{\mathbf{k}} - \mu \equiv k_z^2/2m + 2t[2 - \cos(k_x d) - \cos(k_y d)] - \mu$, where k_z is the momentum in the z direction in the continuum dimension, k_x and k_y are the momenta in the lattice plane, t and d are the hopping integral and lattice constant in the x-y plane, respectively, and μ is the chemical potential. Following our recent works [15,36,40,41], we take t to be physically accessible, under the constraint $2mtd^2 < 1$ in our calculation. The critical coupling for forming a two-body bound state of zero binding energy is given by $U_c^{-1} = -\sum_{\mathbf{k}} 1/2\epsilon_{\mathbf{k}} = -0.16072\sqrt{2m}/\sqrt{t}d^2$. Here and throughout we take natural units and set $\hbar = k_B = 1$. At zero temperature, the mean-field BCS-Leggett ground state follows the gap and number equations [38]

$$0 = \frac{1}{U} + \sum_{\mathbf{k}} \frac{1}{2E_{\mathbf{k}}}, \tag{1}$$

$$n = \sum_{\mathbf{k}} \left(1 - \frac{\xi_{\mathbf{k}}}{E_{\mathbf{k}}}\right), \tag{2}$$

where $E_{\mathbf{k}} = \sqrt{\xi_{\mathbf{k}}^2 + \Delta^2}$ is the Bogoliubov quasiparticle dispersion, with an energy gap Δ.

To make sure the mean-field solution is stable, we impose the requirement that the dispersion of Cooper pairs be nonnegative, both in the lattice plane and in the z direction. To this end, we extract the inverse pair mass (tensor) using the fluctuating pair propagator, as given in the pairing fluctuation theory which was previously developed for the pseudogap physics in the cuprates [42] and extended to address the BCS-BEC crossover in ultracold atomic Fermi gases [1].[1] In particular, we mention that, compared to rival T-matrix approximations for the pairing physics, the pair dispersion as extracted from this theory is gapless below T_c, fully compatible with the mean-field gap equation. Here the pairing T matrix is given by $t_{pg}(Q) = U/[1 + U\chi(Q)]$, with the pair susceptibility $\chi(Q) = \sum_K G_0(Q - K)G(K)$, the bare Green's

[1]Note that it suffices to extract the pair dispersion at the T-matrix level, while there exists a small linear pair dispersion regime in the long-wavelength limit when collective modes and direct pair-pair interactions are taken into account beyond the T-matrix level. Furthermore, it can be shown that this linear regime is small for both weak and strong pairing. For weak pairing, the pair mass is very light [21] and the pair density is very low, while for strong pairing, the interpair interaction becomes weak for short-range pairing interactions so that the coupled collective mode velocity becomes low [43]. One may find a larger linear regime for intermediate pairing strength, if the pairs are energetically stable.

function $G_0(K) = (\omega - \xi_{\mathbf{k}})^{-1}$, and the full Green's function $G(K) = \frac{u_{\mathbf{k}}^2}{\omega - E_{\mathbf{k}}} + \frac{v_{\mathbf{k}}^2}{\omega + E_{\mathbf{k}}}$, where $u_{\mathbf{k}}^2 = (1 + \xi_{\mathbf{k}}/E_{\mathbf{k}})/2$ and $v_{\mathbf{k}}^2 = (1 - \xi_{\mathbf{k}}/E_{\mathbf{k}})/2$ are the BCS coherence factors, and $K \equiv (\omega, \mathbf{k})$ and $Q \equiv (\Omega, \mathbf{q})$ are four momenta.

The inverse T matrix $t_{\rm pg}^{-1}(Q)$ can be expanded for small Q, given by

$$t_{\rm pg}^{-1}(\Omega, \mathbf{q}) \approx a_1 \Omega^2 + a_0(\Omega - \Omega_{\mathbf{q}} + \mu_p),$$

with dispersion $\Omega_{\mathbf{q}} = B{q_z}^2 + 2t_{\rm B}[2 - \cos(q_x d) - \cos(q_y d)]$ and the effective pair chemical potential $\mu_{\rm p} = 0$ in the superfluid phase. Through this expansion, we can extract $B = 1/2M$, with M the effective pair mass in the z direction, and the effective pair hopping integral $t_{\rm B}$ in the x-y plane. The sign of a_0 determines whether the fermion pairs are particlelike or holelike, with positive a_0 for particlelike pairing and negative a_0 for holelike pairing. For example, in a 3D lattice, in general one finds $a_0 > 0$ for fermion density below half filling, $a_0 = 0$ at half filling due to particle-hole symmetry, and $a_0 < 0$ above half filling. The sign of a_0 is controlled by the average of the inverse band mass.[2] While one could perform a particle-hole transformation for a pure lattice case, it does not seem to be feasible in our case since both lattice and continuum dimensions are present. The expressions for the coefficients a_1, a_0, B, and $t_{\rm B}$ can be readily derived during the Taylor expansion. In this way, using the solution for (μ, Δ) from Eqs. (1) and (2), we can extract the pair dispersion $\tilde{\Omega}_{\mathbf{q}} = (\sqrt{a_0^2 + 4a_1 a_0 \Omega_{\mathbf{q}}} - a_0)/2a_1$. The non-negativeness of the pair dispersion implies that the pairing correlation length (squared) $\xi^2 = a_0 B$ and $\xi_{xy}^2 = a_0 t_{\rm B} d^2$ must be positive.

For the population imbalanced case, the spin polarization is defined via $p = (n_\uparrow - n_\downarrow)/(n_\uparrow + n_\downarrow)$, where the spin index $\sigma = \uparrow, \downarrow$ refers to the majority and minority components, respectively. Then the dispersion of noninteracting atoms is modified as $\xi_{\mathbf{k}\sigma} = \epsilon_{\mathbf{k}} - \mu_\sigma$, with μ_σ the chemical potential for spin σ.

Now the bare and full Green's functions are given by

$$G_{0\sigma}(K) = \frac{1}{\omega - \xi_{\mathbf{k}\sigma}},$$

$$G_\sigma(K) = \frac{u_{\mathbf{k}}^2}{\omega - E_{\mathbf{k}\sigma}} + \frac{v_{\mathbf{k}}^2}{\omega + E_{\mathbf{k}\bar{\sigma}}},$$

respectively, where $\bar{\sigma}$ is the opposite spin of σ, $E_{\mathbf{k}\uparrow} = E_{\mathbf{k}} - h$, and $E_{\mathbf{k}\downarrow} = E_{\mathbf{k}} + h$, with the average $\mu = (\mu_\uparrow + \mu_\downarrow)/2$ and the magnetic field $h = (\mu_\uparrow - \mu_\downarrow)/2$. Thus $E_{\mathbf{k}\uparrow}$ becomes gapless, as it should, in order to accommodate the excessive majority fermions [see Eq. (5) below]. These gapless fermions will contribute in both the gap and number equations.

Following the BCS self-consistency condition (i.e., the definition of the order parameter) and the number constraint, we arrive at the gap and number equations at zero T in the presence of population imbalance,

$$0 = \frac{1}{U} + \sum_{\mathbf{k}} \frac{\Theta(E_{\mathbf{k}\uparrow})}{2E_{\mathbf{k}}}, \tag{3}$$

[2]For the latter case, one can perform a particle-hole transformation so that it becomes $a_0 > 0$ and below half filling for holes.

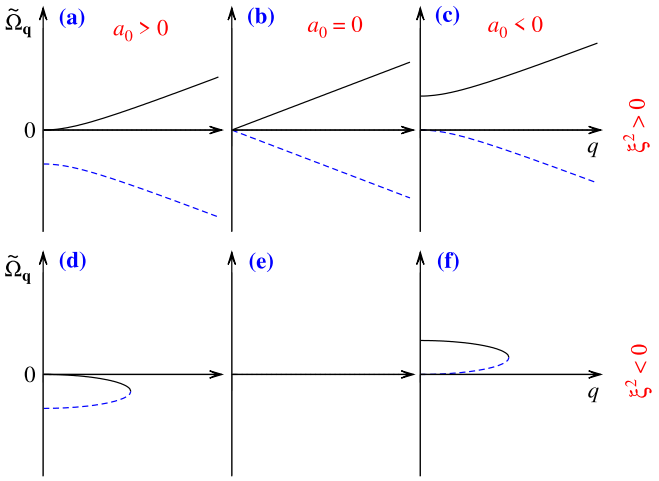

FIG. 1. Qualitative behavior of the pair dispersion $\tilde{\Omega}_{\mathbf{q}}$ for different signs of a_0 and ξ^2: (a) and (d) $a_0 > 0$, (b) and (e) $a_0 = 0$, and (c) and (f) $a_0 < 0$ and (a)–(c) $\xi^2 > 0$ and (d)–(f) $\xi^2 < 0$. For illustrative purposes, a simple isotropic quadratic $\Omega_{\mathbf{q}} = \xi^2 q^2/a_0$ is used. The black solid curves in (a)–(c) represent propagating modes.

$$n = \sum_{\mathbf{k}} \left[\left(1 - \frac{\xi_{\mathbf{k}}}{E_{\mathbf{k}}}\right) + \Theta(-E_{\mathbf{k}\uparrow}) \frac{\xi_{\mathbf{k}}}{E_{\mathbf{k}}} \right], \tag{4}$$

$$pn = \sum_{\mathbf{k}} \Theta(-E_{\mathbf{k}\uparrow}), \tag{5}$$

where $\Theta(x)$ is the Heaviside step function and $n = n_\uparrow + n_\downarrow$ and $\delta n = n_\uparrow - n_\downarrow = pn$ are the total and the difference of fermion densities, respectively. In the imbalanced case, the pair susceptibility is modified as $\chi(Q) = \sum_{K,\sigma} G_{0\sigma}(Q - K) G_{\bar{\sigma}}(K)/2$, which is consistent with the BCS self-consistency condition so that the pair dispersion remains gapless at $q = 0$. Then we follow the same procedure as in the balanced case and extract the inverse pair mass tensor along with coefficients a_0 and a_1 via the Taylor expansion of the inverse T matrix, $t_{\rm pg}^{-1}(Q)$. Equations (3)–(5) form a closed set of self-consistent equations and can be used to solve for (μ, h, Δ) as a function of (U, t, d, p), which is then further constrained by various stability conditions.

B. Stability analysis

As shown in the 3D continuum and 1DOL cases, in the presence of population imbalance, not all solutions of Eqs. (3)–(5) are stable [9,19,44]. Following the stability analysis of Refs. [9,19], the stability condition for the superfluid phase requires that for fixed μ and h, the solution for the excitation gap Δ is a minimum of the thermodynamic potential $\Omega_{\rm S}$, which is demonstrated to be equivalent to the positive definiteness of the generalized compressibility matrix [7,9]. Thus we have

$$\frac{\partial^2 \Omega_{\rm S}}{\partial \Delta^2} = \sum_{\mathbf{k}} \frac{\Delta^2}{E_{\mathbf{k}}^2} \left(\frac{\Theta(E_{\mathbf{k}\uparrow})}{E_{\mathbf{k}}} - \delta(E_{\mathbf{k}\uparrow}) \right) > 0, \tag{6}$$

where $\delta(x)$ is the delta function. In addition, the positivity of the pair dispersion in the entire momentum space imposes another strong stability condition. Illustrated in Fig. 1 are

the qualitative behaviors of the pair dispersion, for different signs of a_0 and ξ^2. For illustrative purposes, a simple isotropic quadratic dispersion is assumed. In general, there are two branches of the dispersion, from the inverse-T-matrix expansion up to the Ω^2 order. The positive branch represents a propagating mode, while the negative branch represents a holelike mode which contributes to quantum fluctuations. The case of $a_0 > 0$ and $\xi^2 > 0$ [Fig. 1(a)] corresponds to particlelike pairing, with a monotonically increasing energy and a positive effective pair mass, $B > 0$ and $t_B > 0$, so that $q = 0$ is the bottom of the pair energy. For the $a_0 < 0$ case [Fig. 1(c)], this dispersion flips upside down into the blue dashed hole mode. This corresponds to holelike pairing, for which $q = 0$ becomes a local maximum, with $B < 0$ and $t_B < 0$, similar to the hole band in a semiconductor. In the case of a pure lattice, one could flip the sign of a_0 via a particle-hole transformation so that this blue dashed line is flipped back to become positive as the dispersion for hole pairs. However, for our present case, due to the presence of the continuum dimension, there is no easy way to do a particle-hole transformation so that we have to stay with the (black solid) gapped positive branch, which is a flip of the hole branch in Fig. 1(a), as the dispersion of particlelike Cooper pairs. When $a_0 = 0$, the two branches become symmetric, without a gap. For all three cases, the coefficients of the q^2 terms in the inverse-T-matrix expansion, ξ^2 and ξ_{xy}^2, must be positive. (Note that a_1 is always positive.) Indeed, as shown in Figs. 1(d)–1(f), for a negative ξ^2, the dispersion $\tilde{\Omega}_{\mathbf{q}}$ of both particlelike [Figs. 1(d)] and holelike [Fig. 1(f)] pairs quickly becomes diffusive and thus ceases to exist, unless higher-order terms, e.g., the q^4 terms, are included. In that case, the pair dispersion will reach a minimum at a nonzero q. Our numerics shows that in a 2DOL, ξ^2 in the continuum dimension remains positive in general but $\xi_{xy}^2 \propto a_0 t_B$ in the lattice plane may indeed change sign so that $\xi_{xy}^2 > 0$ will constitute another stability requirement for the superfluid phase.

Finally, the superfluid density must also be positive definite in a stable superfluid [9,19,45]. This, however, has been found to be a weaker constraint in the cases of a 3D continuum [9,19].

C. Superfluid density

As a representative transport property, superfluid density is an important quantity in the superfluid phase. While it is always given by n/m at zero T for the balanced case in a 3D continuum, it will take the average of the inverse band mass in the presence of a lattice. Furthermore, in the presence of population imbalance, it may become negative [9,19,46], signaling an instability of the superfluid state. Here we also investigate the behavior of the anisotropic superfluid density (n_s/m) and pay close attention to the population imbalanced case and the situations where it becomes negative.

The expression for superfluid density can be derived using the linear-response theory within the BCS framework. The result is identical to that obtained within the pairing fluctuation theory [9,19,42,46–48] at $T = 0$,

$$\left(\frac{n_s}{m}\right)_i = \sum_{\mathbf{k}} \frac{\Delta^2}{E_{\mathbf{k}}^2}\left(\frac{\Theta(E_{\mathbf{k}\uparrow})}{E_{\mathbf{k}}} - \delta(E_{\mathbf{k}\uparrow})\right)\left(\frac{\partial \xi_{\mathbf{k}}}{\partial k_i}\right)^2, \quad (7)$$

where $i = x, y$ and z for the lattice and the continuum directions, respectively.

It should be noted that on a lattice, where the band mass is momentum dependent and thus no longer a constant, one can only define the ratio (n_s/m) as a single variable for the lattice dimensions, without separate definitions of n_s and effective m. (Experimentally, the superfluid density of a superconductor is measured via the London penetration depth [42].) For lattice dimensions the m inside this ratio has no relation to the bare mass from the continuum dimension. At zero T, one may however calculate the average $(1/m)$ for the balanced case by setting $n_s = n$. For the continuum dimension, indeed, we have $(n_s/m)_z = n/m = (2/3\pi^2)k_F E_F$ at zero T.

III. NUMERICAL RESULTS AND DISCUSSION

Due to the multiple tunable parameters for the present 2DOL, the compete multidimensional phase diagram can be extremely complex. Therefore, we focus on the lattice effect for the $p = 0$ case, together with the population imbalance for the $p \neq 0$ case, to give several representative and informative phase diagrams. For our numerics, it is convenient to define the Fermi momentum $k_F = (3\pi^2 n)^{1/3}$ and Fermi energy $E_F \equiv k_B T_F = \hbar^2 k_F^2/2m$ as the units of momentum and energy, respectively, which also sets $2m = 1$. Note, however, that this E_F is *not* equal to the chemical potential in the noninteracting limit.

A. Fermi surfaces in the noninteracting limit

The Fermi surface plays an important role in the superfluid and pairing behavior of atomic Fermi gases. For a 2DOL, it is very different from the 3D continuum or 3D lattice case, as well as from the 1DOL case [15,36,40]. This will lead to different physics. Here we first present the shape and topology of the Fermi surface for a series of representative sets of lattice parameters (t, d). Shown in Fig. 2 is the typical evolution behavior of the Fermi surface, calculated self-consistently in the noninteracting limit at zero temperature. The top row shows the evolution with the lattice constant, for $k_F d = 1, 2, 3$, and 4 at fixed hopping integral $t/E_F = 0.05$. The bottom row shows the effect of the hopping integral with $t/E_F = 0.01, 0.04, 0.07$, and 0.1 and fixed $k_F d = 3$.

The lattice constant d provides a confinement in the momentum space; the larger the d, the stronger the confinement.[3] The top row in Fig. 2 suggests that the Fermi surface becomes thicker along the z direction as d increases for fixed t. Indeed, fermions experience a stronger confinement in the lattice dimensions with a shrinking first Brillouin zone (BZ), as $k_F d$ increases from 1 to 4, and thus need to occupy higher-k_z states to keep the Fermi volume unchanged so that the noninteracting fermionic chemical potential is pushed up. As a rough estimate, the maximum occupied k_z increases by a factor of 16 from left to right. For relatively small $t/E_F = 0.05$, the shape and topology of the Fermi surface evolve from a closed plate for $k_F d = 1$ into one with only the top and bottom faces while completely open on the four sides at the BZ boundary of

[3]The confinement also changes the two-body binding energy.

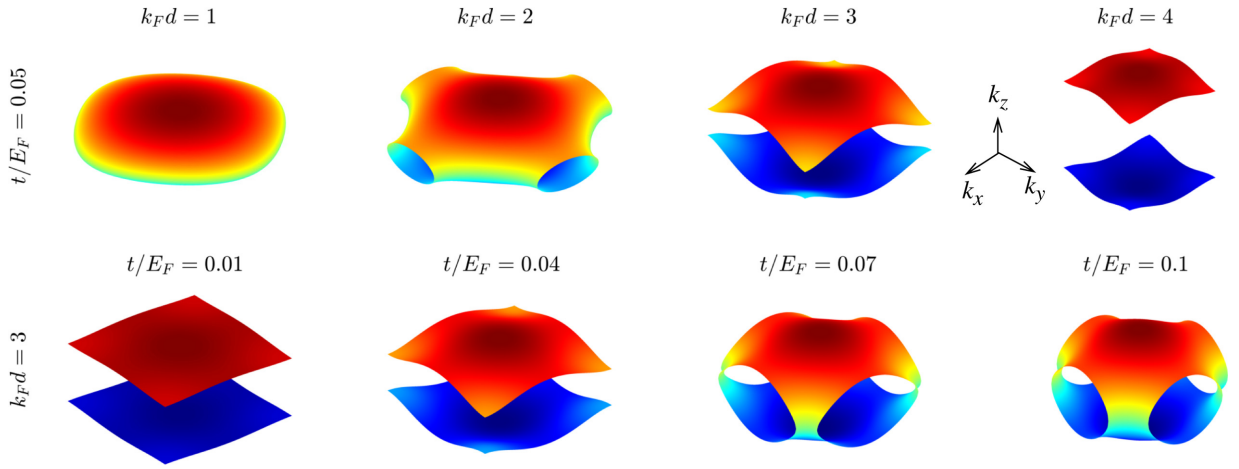

FIG. 2. Evolution of the Fermi surface of atomic Fermi gases in a 2DOL for fixed $t/E_F = 0.05$ (top row) with $k_Fd = 1, 2, 3, 4$, and fixed $k_Fd = 3$ (bottom row) with $t/E_F = 0.01, 0.04, 0.07$, and 0.1, from left to right.

the lattice dimensions for $k_Fd = 3$ and 4. For the intermediate $k_Fd = 2$, the Fermi surface is open only at the center of the four side faces at the BZ boundary. At the same time, the effective filling factor in the lattice dimensions increases to nearly unity as k_Fd increases from 1 to 4. In this way, for large d, fermion dispersion on the Fermi surface on average becomes holelike in the lattice plane, while it always remains particlelike in the continuum dimension.

On the other hand, a smaller t makes the fermion energy less dispersive in the lattice dimensions, and thus the lattice band becomes narrower and more fully filled. In other words, fermions will tend not to go to higher-k_z states until the BZ at lower k_z is fully occupied, leading to a flatter top and bottom of the Fermi surface. This will also pull down the noninteracting fermionic chemical potential. As shown in the bottom row in Fig. 2, the Fermi surface becomes thinner and flatter in the z direction as t/E_F decreases from 0.1 to 0.01 for fixed $k_Fd = 3$. In contrast, the $t/E_F = 0.07$ and 0.1 cases have a much more dispersive Fermi surface as a function of the in-plane momentum (k_x, k_y). Fermions at high-(k_x, k_y) states are removed for relatively large hopping integrals $t/E_F = 0.07$ and 0.1.

The evolution of the Fermi surface reveals that the in-plane fermion motion on the Fermi surface becomes holelike for relatively small t and large d. As a result, the nature of the in-plane and overall pairing in this case will also change from particlelike to holelike when the contributions from lattice dimensions are dominant in the BCS and unitary regimes [37].

It should be mentioned that in the strong-pairing regime, the detailed shape of the Fermi surface is no longer relevant, as pairing extends essentially to the entire momentum space. However, the confinement in the momentum space imposed by the lattice periodicity is always present and will govern the physical behavior in the BEC regime.

B. Phase diagram for the population balanced case

It is known from the 3D continuum case that the balanced case and the imbalanced case with $p \to 0^+$ are not continuously connected in the BCS and unitary regimes at $T = 0$ [19,49]. Population imbalance leads to very distinct behaviors. Therefore, we present in this section the balanced results only.

In Fig. 3 we present a typical phase diagram in the d-U plane [Fig. 3(a)], for fixed relatively small $t/E_F = 0.05$, and in the t-U plane [Fig. 3(b)], for relatively large $k_Fd = 3$, corresponding to the cases of the top and bottom rows in

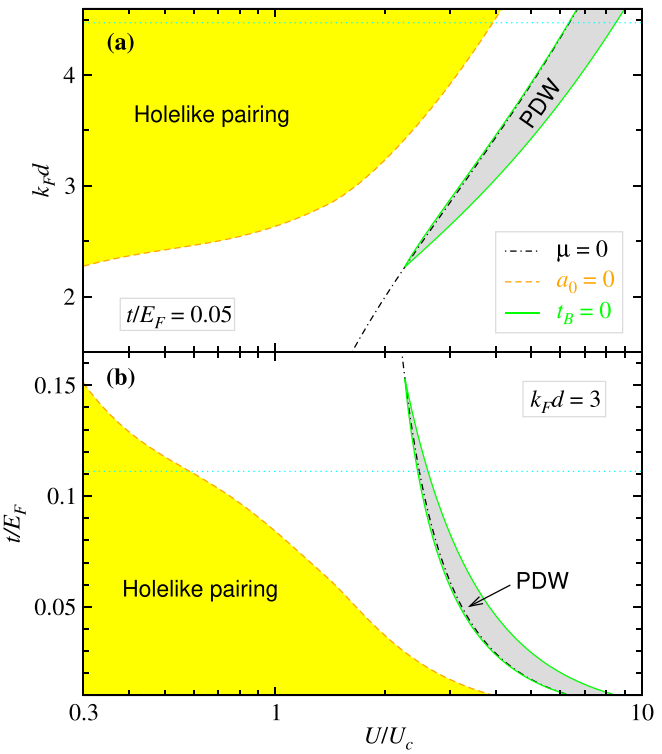

FIG. 3. Phase diagram in the balanced case in (a) the d-U plane for $t/E_F = 0.05$ and (b) the t-U plane for $k_Fd = 3$. The (orange dashed) $a_0 = 0$ curve separates holelike pairing (yellow shaded region) on the left from particlelike pairing on the right. Enclosed inside the (green) $t_B = 0$ line is a pair density wave ground state (gray shaded region). Also plotted is the (black dot-dashed) $\mu = 0$ line. The (cyan) dotted line denotes the upper limit for (a) d and (b) t, as defined by $2mtd^2 \leqslant 1$.

Fig. 2, respectively. The lattice constant in Fig. 3(a) ranges from relatively small $k_F d = 1$ with $2mtd^2 = 0.05$ to the upper limit $k_F d = 2\sqrt{5}$ with $2mtd^2 = 1$ denoted by the horizontal (cyan) dotted line, and the hopping integral in Fig. 3(b) ranges from relatively small $t/E_F = 0.01$ with $2mtd^2 = 0.09$ to the upper limit $t/E_F = 1/9$ with $2mtd^2 = 1$ denoted by the horizontal (cyan) dotted line. In both panels the (black dot-dashed) $\mu = 0$ curve defines the boundary between the fermionic and the bosonic regimes. The (yellow) shaded region on the left of the (orange) dashed $a_0 = 0$ curve is a holelike pairing regime with $a_0 < 0$, whereas the overall pairing evolves from holelike into particlelike with $a_0 > 0$ across the $a_0 = 0$ curve. A PDW ground state with $t_B < 0$ emerges within the gray shaded region, enclosed within the (green) $t_B = 0$ curve. The entire phase space is a superfluid except for the PDW phase. Note that the PDW phase usually starts immediately before μ decreases down to zero, as the pairing strength increases. The fact that there are two branches of the $t_B = 0$ curve indicates that there is a reentrant behavior of T_c as a function of pairing strength. In the absence of population imbalance, similar reentrant behavior of superfluidity and associated PDW ground state have *not* been found in any other balanced systems with a short-range pairing interaction, except in a very narrow range of density slightly above 0.53 in the attractive Hubbard model [48,50,51]. With a long-range anisotropic dipole-dipole interaction, however, such a reentrant behavior and PDW state have been predicted in the p-wave superfluid in dipolar Fermi gases [39].

As shown in Fig. 3, the interaction range for holelike pairing extends toward a stronger-pairing regime with increasing d [Fig. 3(a)] or decreasing t [Fig. 3(b)]. This can be explained by the evolution of the shape and topology of the Fermi surface, as shown in Fig. 2. As d increases or t decreases, the Fermi surface gradually opens up at the four X or Y points located at $(k_x, k_y) = (\pm\pi/d, 0)$ and $(0, \pm\pi/d)$ and becomes fully open at the first BZ boundary for large d and small t, leading to an effective filling factor above $\frac{1}{2}$ in the lattice dimensions. In contrast to the 1DOL case, the existence of two lattice dimensions is enough to dominate the contributions of the remaining one continuum dimension (which is always particlelike due to its parabolic fermion dispersion) so that both the in-plane and overall pairing become holelike when d is large or t is small, with $a_0 < 0$ in the linear frequency term of the inverse-T-matrix expansion. This is especially true in the weak-coupling regime, where the superfluidity is more sensitive to the underlying Fermi surface. As the interaction becomes stronger toward the BEC regime, the gap becomes large and the Fermi level (i.e., chemical potential μ) decreases and then becomes negative; hence the shape of the noninteracting Fermi surface is no longer important. In this case, the contributions from the lattice dimensions will spread evenly across the entire BZ, so that the continuum dimension will become dominant, and the overall pairing eventually changes from holelike to particlelike (with $a_0 > 0$). As shown in Fig. 2, within the occupied range of k_z, the average (or effective) filling factor within the first BZ in the x-y plane increases with increasing d and/or decreasing t. Therefore, as d increases or t decreases, the effect of the above-half-filling status persists into stronger pairing regime and thus the holelike pairing region in Fig. 3 extends toward right.

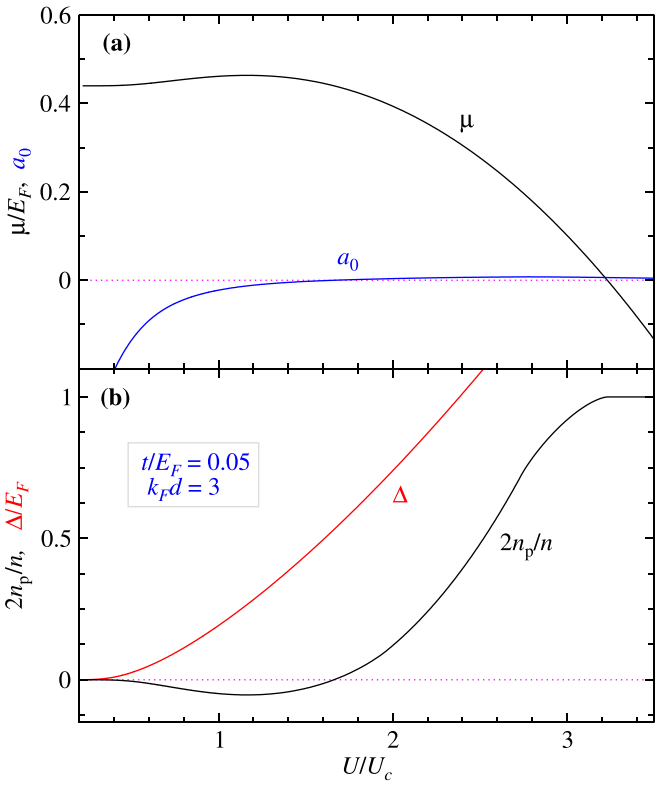

FIG. 4. Behaviors of (a) μ and a_0 and (b) $2n_p/n$ and Δ as a function of U/U_c for $t/E_F = 0.05$ and $k_F d = 3$ without population imbalance. The maximum of μ corresponds to the minimum of the pair fraction $2n_p/n$.

Shown in Fig. 4 is the behavior of μ as a function of U [Fig. 4(a)], along with $2n_p/n$ [Fig. 4(b)], where $n_p \equiv a_0\Delta^2$, for $t/E_F = 0.05$ and $k_F d = 3$. Also plotted are a_0 and Δ. This corresponds to a horizontal cut at $k_F d = 3$ in Fig. 3(a) or at $t/E_F = 0.05$ in Fig. 3(b). Inside the holelike pairing regime, $a_0 < 0$ and thus the chemical potential μ goes above its noninteracting value. This can be seen from the expression [37,48]

$$\sum_{\mathbf{k}} \Theta(-\xi_{\mathbf{k}}) = n/2 - a_0\Delta^2. \tag{8}$$

The chemical potential μ increases with the pairing strength, until it reaches a maximum where n_p reaches a minimum. Here n_p can be roughly understood as the pair density, so $2n_p/n$ is the pair fraction, which reaches unity in the BEC regime. This plot is very close to its counterpart at T_c, which can be found in Ref. [37], since the temperature dependences of both μ and a_0 are weak, except that here a_0 changes sign at a slightly larger U/U_c. As usual, the excitation gap Δ increases with U/U_c.

The PDW ground state in Fig. 3 with $t_B < 0$ at a intermediate-coupling strength for relatively large $k_F d$ with fixed $t/E_F = 0.05$ [Fig. 3(a)] or small t with fixed $k_F d = 3$ [Fig. 3(b)] is associated with the strong interpair repulsive interaction, relatively large pair size, and high pair density. Close to $\mu = 0$, nearly all fermions have paired up with a relatively large pair size and a heavy effective pair mass, and the interpair repulsive interaction becomes strong. A large d or

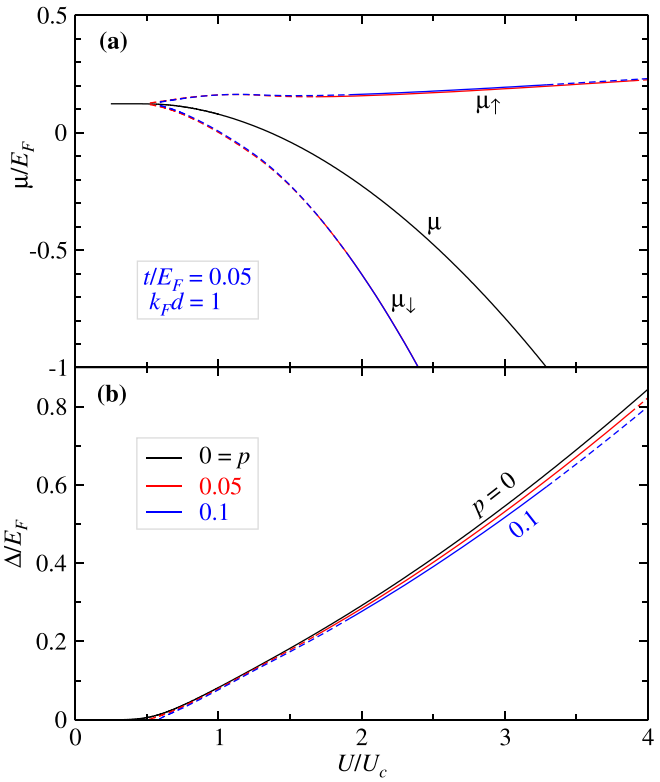

FIG. 5. Behaviors of (a) μ or μ_σ and (b) Δ as a function of U/U_c for $p = 0$ (black lines), 0.05 (red lines), and 0.1 (blue lines), with fixed $t/E_F = 0.05$ and $k_Fd = 1$. Here solid and dashed lines denote stable and unstable solutions, respectively.

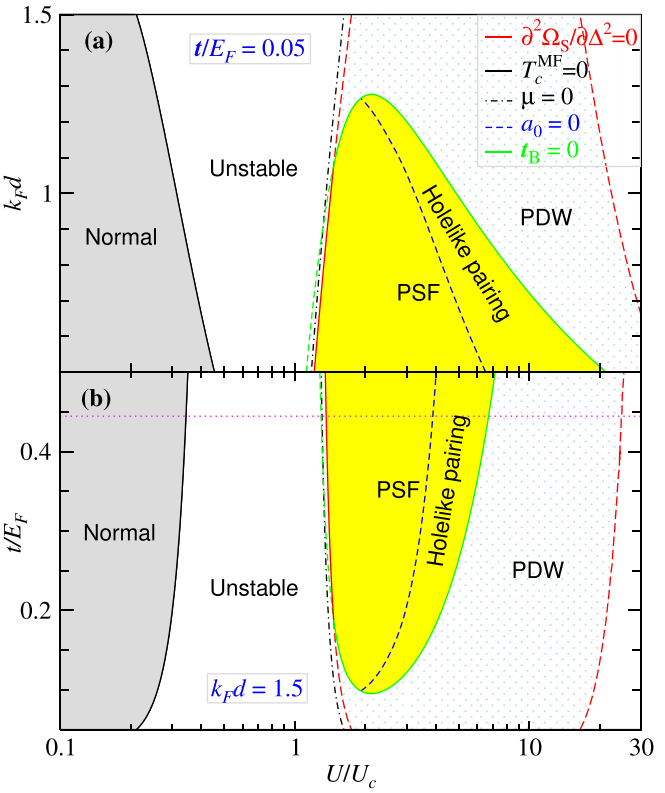

FIG. 6. Phase diagrams at $p = 0.001$ in (a) the d-U plane with $t/E_F = 0.05$ and (b) the t-U plane with $k_Fd = 1.5$. As labeled, the solid lines along with the (red) stability line split the diagram into four phases: normal gas (gray shaded region, on the left of the black $T_c^{MF} = 0$ line), unstable mean-field superfluid (unshaded region), PDW phase (dot shaded region), and stable polarized superfluid (yellow shaded region, bounded by the green $t_B = 0$ line). The pairing on the right of the $a_0 = 0$ (blue dashed) line has a holelike nature. The chemical potential $\mu = 0$ (black dot-dashed) line separates the fermionic regime (on the left) from the bosonic regime (on the right). The (magenta) dotted line sets the upper bound for t via $2mtd^2 \leqslant 1$.

small t strongly suppresses the pairing hopping kinetic energy, and the large pair size and high pair density strongly reduce the pair mobility. All these factors lead to Wigner crystallization and hence PDW in the x-y plane, which can also be called a Cooper pair insulator. The negative sign of t_B within the gray shaded region indicates that the minimum of the pair dispersion $\tilde{\Omega}_{\mathbf{q}}$ has shifted from $\mathbf{q} = 0$ to $\mathbf{q} = (\pi/d, \pi/d, 0)$, with a crystallization wave vector (q_x, q_y) in the x-y plane.[4] An example of the pair dispersion in the PDW state can be found in Fig. 4 of Ref. [37]. As the pairing interaction increases in the BEC regimes, the pair size shrinks and the interpair repulsive interaction becomes weak; hence t_B changes from negative back to positive, corresponding to a quantum phase transition from a PDW insulator to a superfluid.

Combining Figs. 2 and 3, we find that the emergence of holelike pairing and the PDW phase is associated with the open Fermi surface topology. Once the Fermi surface is closed, both holelike pairing and the PDW phase disappear.

In the case of a closed Fermi surface, typical behaviors of the chemical potential μ and the excitation gap Δ for the balanced case can be seen from the $p = 0$ lines in Fig. 5, calculated for $t/E_F = 0.05$ and $k_Fd = 1$. Here μ decreases monotonically with U/U_c. Without a holelike pairing regime, these solutions look qualitatively similar to other cases, e.g., in a 3D continuum or 3D lattice, except that they follow a different asymptotic behavior in the BEC limit [37].

C. Phase diagram for the population imbalanced case

We now proceed and present our results for the population imbalanced case. With the added parameter p, the phase diagram becomes much more complicated. It renders the otherwise superfluid state unstable in the vast areas in the phase space.

To make the comparison easier, we begin by presenting phase diagrams in Fig. 6 in the same d-U [Fig. 6(a)] and t-U [Fig. 6(b)] planes as in Fig. 3 but with a tiny nonzero $p = 0.001$. Here a normal gas phase (gray shaded) emerges in the weak-coupling regime, delineated by the (black solid) $T_c^{MF} = 0$ line, which is given by Eqs. (3)–(5) with $\Delta = 0$. Indeed, in the presence of an imbalance, pairing cannot take place for an arbitrarily weak interaction. There exists a stable PSF phase (yellow shaded region), defined by the (green solid)

[4]Here we use a simple nearest-neighbor tight-binding form as an approximation for the pair dispersion. If higher-order terms are included, the crystallization wave vector could be at different momenta other than $\mathbf{q} = (\pm\pi/d, \pm\pi/d, 0)$.

$t_B = 0$ line and further confined by the stability condition (red solid line). The PSF phase resides in the low-d and large-t regime. A PDW ground state emerges in the dot shaded region, enclosed by the $t_B = 0$ line and the dashed part of the (red) stability line. Then the rest, unshaded space allows for an unstable mean-field superfluid solution, which may yield to phase separation. Now that the underlying lattice in the x-y plane breaks the continuous translational symmetry, the exotic Fulde-Ferrell-Larkin-Ovchinnikov (FFLO) states may possibly exist in part of the unstable region [52–54].

One can immediately tell that the vertical axes in Fig. 6 take different parameter ranges from those in Fig. 3, even though the imbalance $p = 0.001$ is very small. While the d-U phase diagram in Fig. 6(a) is still calculated with $t/E_F = 0.05$, the stable PSF phase is now restricted to relatively small d (yellow shaded area). However, the t-U phase diagram has to be calculated at a much smaller d, with $k_F d = 1.5$, as there is no stable PSF phase for $k_F d = 3$ within the constraint $2mtd^2 \leqslant 1$ (i.e., $t/E_F \leqslant 1/9$). In both cases in Fig. 6, the Fermi surface is closed. Unlike the balanced cases, one cannot find a stable superfluid solution with an open Fermi surface. For this reason, one does not find a holelike pairing region in the weak-coupling regime, but rather one in the strong-coupling regime, on the right of the (blue dashed) $a_0 = 0$ line. Note that in the superfluid phase of holelike pairing (on the right of the blue dashed line), both a_0 and t_B are negative but the product ξ_{xy}^2 is positive. Outside the $t_B = 0$ curve, we have $\xi_{xy}^2 < 0$, so the mean-field superfluid solution becomes unstable, yielding to the PDW phase. The smallness of p suggests that the ground state of $p \to 0^+$ is *not* continuously connected to the $p = 0$ case, consistent with that in the 3D continuum [19]. In comparison with Fig. 3, the current large PDW phase in the bosonic regime is totally a consequence of population imbalance.

Now we take p as a varying parameter and explore phase diagrams in the p-U plane. Shown in Fig. 7 are the phase diagrams for $(t/E_F, k_F d) = (0.15, 1)$ [Fig. 7(a)], $(t/E_F, k_F d) = (0.05, 1)$ [Fig. 7(b)], and $(t/E_F, k_F d) = (0.15, 1.5)$ [Fig. 7(c)]. Figures 7(b) and 7(c) show the effect of changing t and d, respectively. In all three cases, there are three different phases, delineated by solid lines, as well as a PDW phase. A normal gas phase (gray shaded region) takes the weaker-coupling and larger-p area, on the left of the $T_c^{MF} = 0$ curve. The vast majority is an unstable mean-field superfluid (unshaded region), which should yield to phase separation or FFLO solutions. The stable PSF phase (yellow shaded region) occupies only a small area. Finally, the PDW phase (dot shaded region) takes the small region next to the PSF phase, bounded by the (red dashed) stability $\partial^2\Omega_S/\partial\Delta^2 = 0$ line and (green solid) $t_B = 0$ line. When compared with Fig. 7(a), one readily sees that the PSF phase shrinks as t decreases [Fig. 7(b)] and/or as d increases [Fig. 7(c)]. This is because both increasing d and reducing t lead to stronger momentum confinement in the lattice dimensions. In agreement with Fig. 6, the Fermi surface for all these three cases is closed. Note that the (red) stability line and the (green) $t_B = 0$ line cross each other, and the PSF phase is bounded by the stronger of these two conditions. Also plotted here are the lines along which the superfluid density vanishes. As found in the 3D continuum, the positivity of superfluid density constitutes a much weaker stability constraint, as both lines of $(n_s/m)_x = 0$ in the lattice dimension and of $(n_s/m)_z = 0$ in the continuum dimension lie completely within the unstable area. Note that while the $(n_s/m)_z = 0$ line looks very similar to its 3D continuum counterpart, the $(n_s/m)_x = 0$ line exhibits an unusual nonmonotonic behavior,

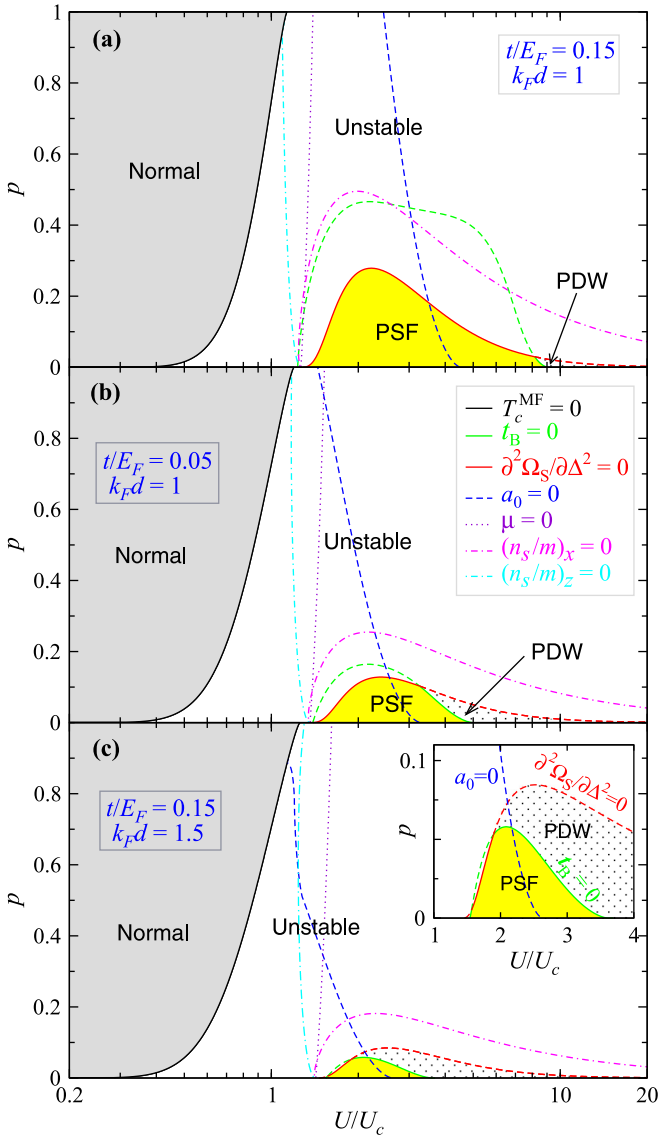

FIG. 7. Phase diagrams in the p-U plane for (a) $(t/E_F, k_F d) = (0.15, 1)$, (b) $(t/E_F, k_F d) = (0.05, 1)$, and (c) $(t/E_F, k_F d) = (0.15, 1.5)$. The solid $T_c^{MF} = 0$ (black) and $t_B = 0$ (green) lines, as well as the (red) stability $\partial^2\Omega_S/\partial\Delta^2 = 0$ line (both solid and dashed) divide the plane into four phases: normal gas (gray shaded region), unstable superfluid (unshaded region), PDW phase (dot shaded region), and stable PSF. Across the $a_0 = 0$ (blue dashed) line the pairing nature changes from particlelike (on the left) to holelike (on the right). The $\mu = 0$ (violet dotted) line separates fermionic (left) from bosonic (right) regimes. Also plotted are lines of the superfluid density $(n_s/m)_x = 0$ (magenta dot-dashed line) in the x direction and $(n_s/m)_z = 0$ (cyan dot-dashed line) in the z direction. The superfluid density is negative on the weaker-coupling or larger-p side of these curves. Shown in the inset of (c) is a close-up of the PSF phase.

caused by the lattice effect. From the (violet dotted) $\mu = 0$ curve, one readily sees that, as in Fig. 6, the PSF phase resides completely within the bosonic regime.

The fact that the PSF phase exists only in a small bosonic region (in both Figs. 6 and 7) is in stark contrast with the 3D continuum case, for which the stability line $\partial^2\Omega_S/\partial\Delta^2 = 0$ extends monotonically up to $p = 1$, and a polarized superfluid exists for arbitrary imbalance p in the BEC regime [19]. Apparently, this difference can be attributed to the presence of two lattice dimensions. Indeed, for a 1DOL, with only one lattice dimension, the stability line already cannot extend to $p = 1$. However, the PSF phase in the 1DOL can extend all the way to the deep BEC limit [44]. This is also supported by the fact that with three lattice dimensions in a 3D attractive Hubbard model, one can barely find a PSF state except at very low density and extremely low p [55]. Therefore, one can conclude that more lattice dimensions makes it more difficult to have a stable PSF ground state.

This phenomenon can be easily understood from the momentum distribution of paired fermions, which would be given by $v_{\mathbf{k}}^2$ had there been no imbalance. In the 3D continuum, $v_{\mathbf{k}}^2$ in the deep BEC regime extends to the entire infinitely large momentum space in all directions, leading to a vanishingly small occupation for paired fermions. Therefore, the excessive majority fermions can readily occupy the low momentum states, with essentially no Pauli blocking from paired fermions. However, when one or more lattice dimensions are present, the momentum in these dimensions is restricted to the first BZ, so that $v_{\mathbf{k}}^2$ in these dimensions cannot be infinitesimally small even in the extreme BEC limit, which will cause a repulsion with excessive majority fermions. This repulsion increases with p and may become costly enough so as to render the mean-field superfluid solution unstable. As a result, the distribution of paired fermions is now roughly given by that of the minority fermions, $n_{\mathbf{k}\downarrow} = \Theta(E_{\mathbf{k}\uparrow})v_{\mathbf{k}}^2$, which reduces to $v_{\mathbf{k}}^2$ for $p = 0$.

Unlike the $p = 0$ case, for which holelike pairing takes place in the weaker-coupling regime when t is small and/or d is large, here holelike pairing occurs in the BEC regime via a completely different mechanism. As mentioned above, all three cases shown in Fig. 7 have a closed noninteracting Fermi surface. As the pairing becomes stronger, the momentum distribution of $v_{\mathbf{k}}^2$ in the x-y plane extends to the entire first BZ and becomes roughly a constant at strong coupling; in the absence of population imbalance, this would lead to a rough cancellation (via averaging over the inverse fermion band mass) due to the particle-hole symmetry of the lattice band. However, for any finite p, the excessive majority fermions will tend to occupy the low-(k_x, k_y) states and thus expel paired fermions toward higher (k_x, k_y) states, which have a negative (i.e., holelike) band mass, leading to a net holelike contribution to a_0 in the pair propagator, when integrated over the entire BZ. This also explains why the $a_0 = 0$ line leans toward weaker coupling with increasing p.

Shown in Fig. 8 is an example of the momentum distributions of $v_{\mathbf{k}}^2$ (left column), $n_{\mathbf{k}\downarrow}$ (middle column), and $\delta n_{\mathbf{k}}$ (right column) in the (k_x, k_y) plane at $k_z/k_F = 0$ (top row), $k_z/k_F = 0.2$ (middle row), and $k_z/k_F = 0.4$ (bottom row), with $U/U_c = 4$ and $p = 0.05$, for $t/E_F = 0.15$ and $k_F d = 1.5$. This corresponds to a PDW state in Fig. 7(c). Indeed, the excessive fermion distribution $\delta n_{\mathbf{k}} = \Theta(-E_{\mathbf{k}\uparrow})$ occupies the low in-plane momentum part and below $k_z/k_F = 0.4$ (right column). In addition, $v_{\mathbf{k}}^2$ (left column) remains roughly constant in the entire BZ and for $|k_z/k_F| \leqslant 0.4$. Most interestingly, the minority fermion distribution $n_{\mathbf{k}\downarrow}$ (middle column) is given by $v_{\mathbf{k}}^2$ but with a hole dug out at the center, due to the Pauli repulsion with the excessive fermions.

As a representative example, we show in Fig. 5 the behavior of μ_σ [Fig. 5(a)] and the gap Δ [Fig. 5(b)] for $p = 0.05$ (red line) and 0.1 (blue line) with fixed $t/E_F = 0.05$ and $k_F d = 1$, as a function of U. They correspond to horizontal cuts at $p = 0.05$ and 0.1 in Fig. 7(b) and should be compared with the $p = 0$ case (black solid curves). The solid parts of these lines are stable PSF solutions, while the dashed lines are unstable mean-field solutions. There are a few remarkable features. First, the excitation gap changes only slowly with imbalance p, except that it does not have a solution below a certain threshold of interaction strength. Second, at a given pairing strength, the μ_σ for $p = 0.05$ and 0.1 are very close to each other, but both far separated from the μ curve for $p = 0$. This again indicates that the $p \to 0^+$ case is not continuously connected to the $p = 0$ case; with a tiny bit of imbalance, $\mu_\uparrow$ and $\mu_\downarrow$ immediately split up. Finally, $\mu_\uparrow$ increases slowly with pairing strength in the BEC regime. This is different from its counterpart in the 3D continuum and 1DOL; for the former $\mu_\uparrow$ decreases, while for the latter $\mu_\uparrow$ approaches a p-dependent constant asymptote, as the pairing strength increases toward the BEC limit. This can be attributed to the emergence of holelike pairing (with $a_0 < 0$) in the strong-pairing regime as the number of lattice dimensions increases. To verify this idea, we have also checked the mean-field solution for an imbalanced 3DOL and found that, indeed, $\mu_\uparrow$ also increases with the pairing strength in the BEC regime at $T = 0$, along with a negative a_0.

Finally, we present the typical behavior of the superfluid density in the imbalanced case. Shown in Fig. 9 are $(n_s/m)_z$ [Fig. 9(a)] and $(n_s/m)_x$ [Fig. 9(b)] in the continuum and lattice dimensions, respectively, as a function of U/U_c for $p = 0$, 0.05, and 0.1 at fixed $t/E_F = 0.05$ and $k_F d = 1$. Here solid and dashed lines are stable and unstable solutions, respectively. As expected, both are always positive for the balanced case. In addition, $(n_s/m)_x$ is much smaller than $(n_s/m)_z$, because it involves the average of the inverse band mass. Note that $(n_s/m)_z = n/m \approx 0.0675(k_F E_F)$, as expected. For the imbalanced case, the superfluid density deviates continuously from its positive $p = 0$ value as p increases from 0. However, in the unitary and weak-coupling regimes, both continuum and lattice components will become negative for $p \neq 0$. Furthermore, the superfluid density is more negative for smaller (but finite) p. This implies an immediate discontinuous jump from the $p = 0$ value to a large negative value for $p = 0^+$ in this regime. Note that for strong enough interaction, $(n_s/m)_x$ will again change sign to negative, but gradually rather than abruptly, as can already be seen from the $p = 0.1$ curve. This has to do with the lattice-induced confinement in the momentum space and the Pauli exclusion between paired and excessive fermions.

So far, it is not yet clear whether the PDW state can sustain a superfluid order, with and without an imbalance. If the answer is that it can, then it will become a supersolid state

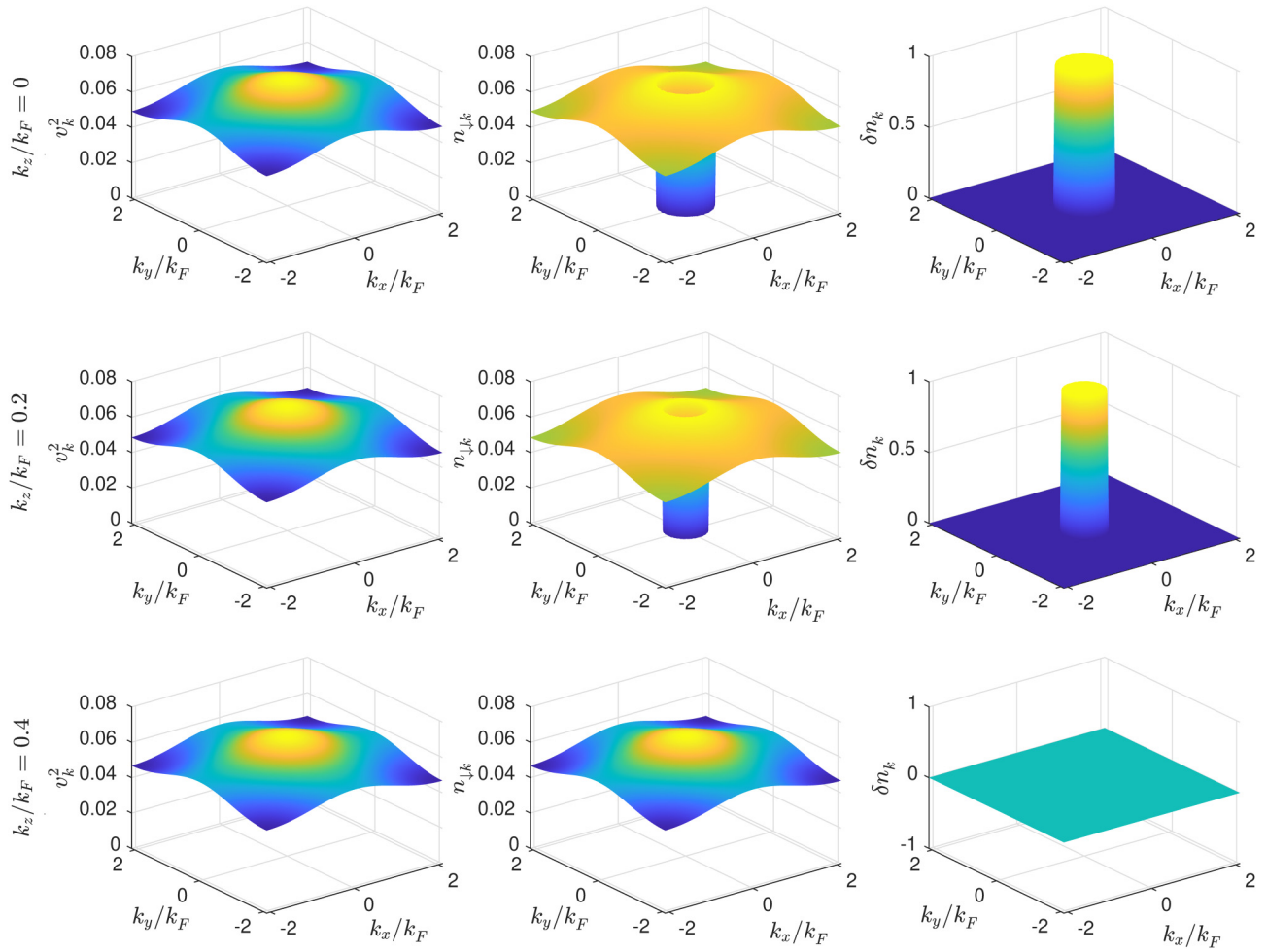

FIG. 8. Momentum distributions of $v_{\mathbf{k}}^2$ (left column), $n_{\mathbf{k}\downarrow}$ (middle column), and $\delta n_{\mathbf{k}}$ (right column) in the (k_x, k_y) plane at $k_z/k_{\mathrm{F}} = 0$ (top row), $k_z/k_{\mathrm{F}} = 0.2$ (middle row), and $k_z/k_{\mathrm{F}} = 0.4$ (bottom row), with $U/U_{\mathrm{c}} = 4$ and $p = 0.05$, for $t/E_{\mathrm{F}} = 0.15$ and $k_{\mathrm{F}}d = 1.5$. The excessive fermion distribution $\delta n_{\mathbf{k}}$ occupies the low in-plane momentum part and below $k_z/k_{\mathrm{F}} = 0.4$ (right column), $v_{\mathbf{k}}^2$ (left column) remains roughly constant in the entire BZ and for $|k_z/k_{\mathrm{F}}| \leqslant 0.4$, and $n_{\mathbf{k}\downarrow}$ (middle column) is given by $v_{\mathbf{k}}^2$ but with the central part expelled.

rather than a Cooper pair insulator. Other issues include how the wave vector of the PDW evolves with various parameters. The exact solution of the PDW state will require a new theory that is beyond the scope of the present work. We leave this to a future study.

It should be noted that we have worked with a system with homogeneous fixed densities. For this reason, we have not chosen to use μ and h as control variables, which are more appropriate for systems connected with a large reservoir so that the chemical potentials are fixed or can be tuned separately. In such a case, all $h < \sqrt{\min(0, \mu)^2 + \Delta^2}$ correspond to the population balanced state. One can, however, convert between these two approaches, by calculating corresponding densities (and Fermi energy) for given μ and h and performing a rescaling.

Finally, we mention that the polaron physics [31,32,56,57] is partially included in the BCS–mean-field-like treatment, in that the Hartree self-energy has been absorbed in the fermion chemical potential μ_σ [see Eq. (2.4) in Ref. [48]]. While this chemical potential does determine the location of the Fermi surface in momentum space, it however differs from the physical chemical potential by the Hartree energy. The treatment of fermion mass renormalization as done in the polaron physics goes beyond the mean-field level of the current BCS-Leggett formalism, despite that it can be readily calculated using a T-matrix approach. Nevertheless, we emphasize that the polaron physics is most relevant at extreme high imbalance, whereas the stable polarized superfluid and PDW state of interest are mainly in the low imbalance regime (Fig. 7), where the polaron physics is not expected to play an important role.

IV. CONCLUSION

In summary, we have studied the superfluid phase diagram of Fermi gases with a short-range pairing interaction in a 2DOL at zero temperature with and without population imbalance in the context of BCS-BEC crossover. We found that the mixing of lattice and continuum dimensions, together with population imbalance, has an extraordinary effect on pairing and the superfluidity of atomic Fermi gases. For the balanced case, the ground state is a stable superfluid, except that a PDW ground state emerges for a finite range of intermediate pairing strength in the case of relatively small t and large d, and the

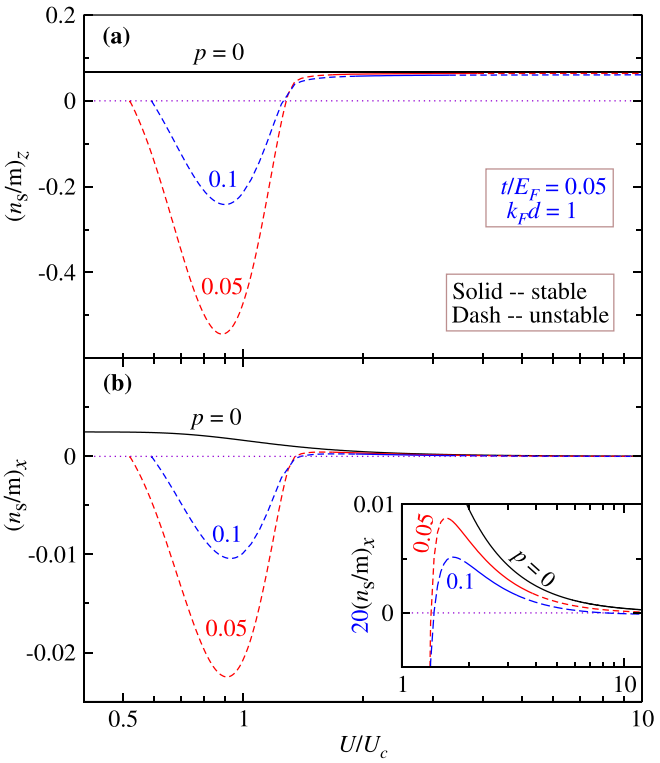

FIG. 9. Superfluid densities (a) $(n_s/m)_z$ and (b) $(n_s/m)_x$, in units of $k_F E_F$, as a function of U/U_c for $p = 0$ (black line), $p = 0.05$ (red line), and $p = 0.1$ (blue line) at $t/E_F = 0.05$ and $k_F d = 1$. Solid (dashed) lines denote stable (unstable) solutions. Shown in the inset is 20 times magnified $(n_s/m)_x$ vs U/U_c. Note that for $p = 0$, $(n_s/m)_z = n/m$ at $T = 0$.

nature of the in-plane and overall pairing may change from particlelike to holelike in the BCS and unitary regimes for these t and d, which are associated with an open Fermi surface on the BZ boundary of the lattice dimensions. Thus the phase space for the PDW ground state and holelike pairing shrinks with increasing t and/or decreasing d.

For the imbalanced case, the presence of population imbalance has a dramatic detrimental effect, in that the stable polarized superfluid phase occupies only a small region in the bosonic regime in the multidimensional phase space and will shrink and disappear with increasing d and p and decreasing t. The PSF phase can be found only for relatively large t and small d, associated with a closed noninteracting Fermi surface, as well as for low p. In comparison with the 3D continuum, the presence of lattice dimensions introduces confinement in the momentum space, which leads to strong Pauli repulsion between paired and excessive fermions. Due to this repulsion, the nature of pairing changes from particlelike to holelike in the strong-pairing regime and a PDW phase emerges next to the PSF phase. In addition to the normal gas phase, stability analysis shows that an unstable mean-field solution exists and may yield to phase separation (and possibly FFLO states) in the rest of the phase diagram.

These findings for the 2DOL are very different from pure 3D continua, 3D lattices, and 1DOLs and should be tested in future experiments. The momentum distributions of both fermion spin components may be detected using spin-selective momentum-resolved rf spectroscopy [58,59]. Precision momentum-resolved rf spectroscopy may also help measure the quasiparticle dispersion and the pairing gap and detect the movement of the Fermi level with the interaction strength in the holelike pairing regime [60]. The pair momentum distribution and pair fraction may be detected using time-of-flight measurements, for which, in both the superfluid and PDW phases, magnetic-field sweep may be needed [61,62]. A maximum of pair distribution at a nonzero in-plane momentum will be support for the PDW phase. The Fermi surface and its topology may be detected with the fermion band-mapping technique [17]. One may also explore the unstable phases using *in situ* imaging techniques to probe possible phase separation [63]. A vortex experiment may also be done to delineate possible superfluid regions in the phase diagrams [4].

ACKNOWLEDGMENTS

This work was supported by the National Natural Science Foundation of China (Grant No. 11774309), the Innovation Program for Quantum Science and Technology (Grant No. 2021ZD0301904), and the University of Science and Technology of China.

[1] Q. J. Chen, J. Stajic, S. N. Tan, and K. Levin, BCS–BEC crossover: From high temperature superconductors to ultracold superfluids, Phys. Rep. **412**, 1 (2005).
[2] I. Bloch, J. Dalibard, and W. Zwerger, Many-body physics with ultracold gases, Rev. Mod. Phys. **80**, 885 (2008).
[3] C. Chin, R. Grimm, P. Julienne, and E. Tiesinga, Feshbach resonances in ultracold gases, Rev. Mod. Phys. **82**, 1225 (2010).
[4] M. W. Zwierlein, A. Schirotzek, C. H. Schunck, and W. Ketterle, Fermionic superfluidity with imbalanced spin populations, Science **311**, 492 (2006).
[5] G. B. Partridge, W. Li, R. I. Kamar, Y.-a. Liao, and R. G. Hulet, Pairing and phase separation in a polarized Fermi gas, Science **311**, 503 (2006).
[6] M. M. Forbes, E. Gubankova, W. V. Liu, and F. Wilczek, Stability Criteria for Breached-Pair Superfluidity, Phys. Rev. Lett. **94**, 017001 (2005).
[7] C.-H. Pao, S.-T. Wu, and S.-K. Yip, Superfluid stability in the BEC-BCS crossover, Phys. Rev. B **73**, 132506 (2006).
[8] W. Yi and L.-M. Duan, Trapped fermions across a Feshbach resonance with population imbalance, Phys. Rev. A **73**, 031604(R) (2006).
[9] Q. J. Chen, Y. He, C.-C. Chien, and K. Levin, Stability conditions and phase diagrams for two-component Fermi gases with population imbalance, Phys. Rev. A **74**, 063603 (2006).
[10] T. N. De Silva and E. J. Mueller, Profiles of near-resonant population-imbalanced trapped Fermi gases, Phys. Rev. A **73**, 051602(R) (2006).
[11] M. Haque and H. T. C. Stoof, Pairing of a trapped resonantly interacting fermion mixture with unequal spin populations, Phys. Rev. A **74**, 011602(R) (2006).
[12] L. Radzihovsky and D. E. Sheehy, Imbalanced Feshbach-resonant Fermi gases, Rep. Prog. Phys. **73**, 076501 (2010).

[13] K. Martiyanov, V. Makhalov, and A. Turlapov, Observation of a Two-Dimensional Fermi Gas of Atoms, Phys. Rev. Lett. **105**, 030404 (2010).

[14] C.-T. Wu, B. M. Anderson, R. Boyack, and K. Levin, Quasicondensation in Two-Dimensional Fermi Gases, Phys. Rev. Lett. **115**, 240401 (2015).

[15] L. F. Zhang, Y. M. Che, J. B. Wang, and Q. J. Chen, Exotic superfluidity and pairing phenomena in atomic Fermi gases in mixed dimensions, Sci. Rep. **7**, 1 (2017).

[16] I. Bloch, Ultracold quantum gases in optical lattices, Nat. Phys. **1**, 23 (2005).

[17] M. Köhl, H. Moritz, T. Stöferle, K. Günter, and T. Esslinger, Fermionic Atoms in a Three Dimensional Optical Lattice: Observing Fermi Surfaces, Dynamics, and Interactions, Phys. Rev. Lett. **94**, 080403 (2005).

[18] U. Schneider, L. Hackermüller, S. Will, T. Best, I. Bloch, T. A. Costi, R. Helmes, D. Rasch, and A. Rosch, Metallic and insulating phases of repulsively interacting fermions in a 3D optical lattice, Science **322**, 1520 (2008).

[19] C.-C. Chien, Q. J. Chen, Y. He, and K. Levin, Intermediate-Temperature Superfluidity in an Atomic Fermi Gas with Population Imbalance, Phys. Rev. Lett. **97**, 090402 (2006).

[20] P. Noziéres and S. Schmitt-Rink, Bose condensation in an attractive fermion gas: From weak to strong coupling superconductivity, J. Low Temp. Phys. **59**, 195 (1985).

[21] Q. J. Chen, I. Kosztin, B. Jankó, and K. Levin, Superconducting transitions from the pseudogap state: d-wave symmetry, lattice, and low-dimensional effects, Phys. Rev. B **59**, 7083 (1999).

[22] V. L. Berezinskii, Destruction of long-range order in one dimensional and two dimensional systems possessing a continuous symmetry group II. Quantum systems, Zh. Eksp. Teor. Fiz. **61**, 1144 (1971) [Sov. Phys. JETP **34**, 610 (1972)]; J. M. Kosterlitz and D. J. Thouless, Ordering, metastability and phase transitions in two dimensional systems, J. Phys. C **6**, 1181 (1973).

[23] A. T. Sommer, L. W. Cheuk, M. J. H. Ku, W. S. Bakr, and M. W. Zwierlein, Evolution of Fermion Pairing from Three to Two Dimensions, Phys. Rev. Lett. **108**, 045302 (2012).

[24] Y.-a. Liao, A. S. C. Rittner, T. Paprotta, W. Li, G. B. Partridge, R. G. Hulet, S. K. Baur, and E. J. Mueller, Spin-imbalance in a one-dimensional Fermi gas, Nature (London) **467**, 567 (2010).

[25] G. Pagano, M. Mancini, G. Cappellini, P. Lombardi, F. Schäfer, H. Hu, X.-J. Liu, J. Catani, C. Sias, M. Inguscio, and L. Fallani, A one-dimensional liquid of fermions with tunable spin, Nat. Phys. **10**, 198 (2014).

[26] M. C. Revelle, J. A. Fry, B. A. Olsen, and R. G. Hulet, 1D to 3D Crossover of a Spin-Imbalanced Fermi gas, Phys. Rev. Lett. **117**, 235301 (2016)>.

[27] C. Cheng, J. Kangara, I. Arakelyan, and J. E. Thomas, Fermi gases in the two-dimensional to quasi-two-dimensional crossover, Phys. Rev. A **94**, 031606(R) (2016).

[28] L. Sobirey, H. Biss, N. Luick, M. Bohlen, H. Moritz, and T. Lompe, Comparing fermionic superfluids in two and three dimensions, arXiv:2106.11893

[29] M. G. Ries, A. N. Wenz, G. Zürn, L. Bayha, I. Boettcher, D. Kedar, P. A. Murthy, M. Neidig, T. Lompe, and S. Jochim, Observation of Pair Condensation in the Quasi-2D BEC-BCS Crossover, Phys. Rev. Lett. **114**, 230401 (2015).

[30] P. A. Murthy, I. Boettcher, L. Bayha, M. Holzmann, D. Kedar, M. Neidig, M. G. Ries, A. N. Wenz, G. Zürn, and S. Jochim, Observation of the Berezinskii-Kosterlitz-Thouless Phase Transition in an Ultracold Fermi Gas, Phys. Rev. Lett. **115**, 010401 (2015).

[31] M. Koschorreck, D. Pertot, E. Vogt, B. Fröhlich, M. Feld, and M. Köhl, Attractive and repulsive Fermi polarons in two dimensions, Nature (London) **485**, 619 (2012).

[32] W. Ong, C. Cheng, I. Arakelyan, and J. E. Thomas, Spin-Imbalanced Quasi-Two-Dimensional Fermi Gases, Phys. Rev. Lett. **114**, 110403 (2015).

[33] D. Mitra, P. T. Brown, P. Schauß, S. S. Kondov, and W. S. Bakr, Phase Separation and Pair Condensation in a Spin-Imbalanced 2D Fermi Gas, Phys. Rev. Lett. **117**, 093601 (2016).

[34] B. C. Mulkerin, L. He, P. Dyke, C. J. Vale, X.-J. Liu, and H. Hu, Superfluid density and critical velocity near the Berezinskii-Kosterlitz-Thouless transition in a two-dimensional strongly interacting Fermi gas, Phys. Rev. A **96**, 053608 (2017).

[35] K. Hueck, N. Luick, L. Sobirey, J. Siegl, T. Lompe, and H. Moritz, Two-Dimensional Homogeneous Fermi Gases, Phys. Rev. Lett. **120**, 060402 (2018).

[36] J. B. Wang, L. Sun, Q. Zhang, L. F. Zhang, Y. Yu, C. H. Lee, and Q. J. Chen, Superfluidity and pairing phenomena in ultracold atomic Fermi gases in one-dimensional optical lattices. II. Effects of population imbalance, Phys. Rev. A **101**, 053618 (2020).

[37] L. Sun, J. B. Wang, X. Chu, and Q. J. Chen, Pairing phenomena and superfluidity of atomic Fermi gases in a two-dimensional optical lattice: Unusual effects of lattice-continuum mixing, Ann. Phys. (Berlin) **534**, 2100511 (2022).

[38] A. J. Leggett, Diatomic molecules and Cooper pairs, in *Modern Trends in the Theory of Condensed Matter*, Lecture Notes in Physics, Vol. 115, edited by A. Pękalski and J. A. Przystawa (Springer, Berlin, 1980), pp. 13–27, proceedings of the XVI Karpacz Winter School of Theoretical Physics, February 19 -March 3, 1979, Karpacz, Poland.

[39] Y. M. Che, J. B. Wang, and Q. J. Chen, Reentrant superfluidity and pair density wave in single-component dipolar Fermi gases, Phys. Rev. A **93**, 063611 (2016).

[40] J. B. Wang, L. F. Zhang, Y. Yu, C. H. Lee, and Q. J. Chen, Superfluidity and pairing phenomena in ultracold atomic Fermi gases in one-dimensional optical lattices. I. Balanced case, Phys. Rev. A **101**, 053617 (2020).

[41] L. F. Zhang, J. B. Wang, Y. Yu, and Q. J. Chen, Ultra high temperature superfluidity in ultracold atomic Fermi gases with mixed dimensionality, Sci. China Phys. Mech. Astron. **63**, 227421 (2020).

[42] Q. J. Chen, I. Kosztin, B. Jankó, and K. Levin, Pairing Fluctuation Theory of Superconducting Properties in Underdoped to overdoped Cuprates, Phys. Rev. Lett. **81**, 4708 (1998).

[43] I. Kosztin, Q. J. Chen, Y.-J. Kao, and K. Levin, Pair excitations, collective modes and gauge invariance in the BCS–Bose-Einstein crossover scenario, Phys. Rev. B **61**, 11662 (2000).

[44] Q. J. Chen, J. B. Wang, L. Sun, and Y. Yu, Unusual destruction and enhancement of superfluidity of atomic Fermi gases by population imbalance in a one-dimensional optical lattice, Chin. Phys. Lett. **37**, 053702 (2020).

[45] L. He, M. Jin, and P. Zhuang, Finite-temperature phase diagram of a two-component Fermi gas with density imbalance, Phys. Rev. B **74**, 214516 (2006).

[46] Y. He, C.-C. Chien, Q. J. Chen, and K. Levin, Thermodynamics and superfluid density in BCS-BEC crossover with and without population imbalance, Phys. Rev. B **76**, 224516 (2007).

[47] I. Kosztin, Q. J. Chen, B. Jankó, and K. Levin, Relationship between the pseudo- and superconducting gaps: Effects of residual pairing correlations below T_c, Phys. Rev. B **58**, R5936 (1998).

[48] Q. J. Chen, Generalization of BCS theory to short coherence length superconductors: A BCS-Bose-Einstein crossover scenario, Ph.D. thesis, University of Chicago, 2000; see also arXiv:1801.06266.

[49] Q. J. Chen, Y. He, C.-C. Chien, and K. Levin, Theory of superfluids with population imbalance: Finite-temperature and BCS-BEC crossover effects, Phys. Rev. B **75**, 014521 (2007).

[50] C.-C. Chien, Y. He, Q. J. Chen, and K. Levin, Superfluid-insulator transitions at noninteger filling in optical lattices of fermionic atoms, Phys. Rev. A **77**, 011601(R) (2008).

[51] C.-C. Chien, Q. J. Chen, and K. Levin, Fermions with attractive interactions on optical lattices and implications for correlated systems, Phys. Rev. A **78**, 043612 (2008).

[52] P. Fulde and R. A. Ferrell, Superconductivity in a strong spin-exchange field, Phys. Rev. **135**, A550 (1964). A. I. Larkin and Y. N. Ovchinnikov, Inhomogeneous state of superconductors, Zh. Eksp. Teor. Fiz. **47**, 1136 (1964) [Sov. Phys. JETP **20**, 762 (1965)].

[53] J. B. Wang, Y. M. Che, L. F. Zhang, and Q. J. Chen, Instability of Fulde-Ferrell-Larkin-Ovchinnikov states in three and two dimensions, Phys. Rev. B **97**, 134513 (2018).

[54] K. V. Samokhin and M. S. Mar'enko, Quantum fluctuations in Larkin-Ovchinnikov-Fulde-Ferrell superconductors, Phys. Rev. B. **73**, 144502 (2006).

[55] A. Cichy and R. Micnas, The spin-imbalanced attractive Hubbard model in $d = 3$: Phase diagrams and BCS-BEC crossover at low filling, Ann. Phys. (NY) **347**, 207 (2014).

[56] F. Chevy, Universal phase diagram of a strongly interacting Fermi gas with unbalanced spin populations, Phys. Rev. A **74**, 063628 (2006).

[57] M. W. Zwierlein, C. H. Schunck, A. Schirotzek, and W. Ketterle, Direct observation of the superfluid phase transition in ultracold Fermi gases, Nature (London) **442**, 54 (2006).

[58] J. T. Stewart, J. P. Gaebler, and D. S. Jin, Using photoemission spectroscopy to probe a strongly interacting Fermi gas, Nature (London) **454**, 744 (2008).

[59] P. Wang, Z.-Q. Yu, Z. Fu, J. Miao, L. Huang, S. Chai, H. Zhai, and J. Zhang, Spin-Orbit Coupled Degenerate Fermi Gases, Phys. Rev. Lett. **109**, 095301 (2012).

[60] J. Gaebler, J. Stewart, T. Drake, D. Jin, A. Perali, P. Pieri, and G. Strinati, Observation of pseudogap behaviour in a strongly interacting Fermi gas, Nat. Phys. **6**, 569 (2010).

[61] C. A. Regal, M. Greiner, and D. S. Jin, Observation of Resonance Condensation of Fermionic Atom Pairs, Phys. Rev. Lett. **92**, 040403 (2004).

[62] T. Paintner, D. K. Hoffmann, M. Jäger, W. Limmer, W. Schoch, B. Deissler, M. Pini, P. Pieri, G. C. Strinati, C. Chin, and J. H. Denschlag, Pair fraction in a finite-temperature Fermi gas on the BEC side of the BCS-BEC crossover, Phys. Rev. A **99**, 053617 (2019).

[63] Y. Shin, M. W. Zwierlein, C. H. Schunck, A. Schirotzek, and W. Ketterle, Observation of Phase Separation in a Strongly Interacting Imbalanced Fermi Gas, Phys. Rev. Lett. **97**, 030401 (2006).